TECHNICAL RESEARCH REPORT

A Simple Control Law for UAV Formation Flying

by E.W. Justh, P.S. Krishnaprasad

TR 2002-38

A Simple Control Law for UAV Formation Flying [*]

E. W. Justh [a] P. S. Krishnaprasad [b]

[a]*Institute for Systems Research*
University of Maryland
College Park, MD 20742, USA

[b]*Institute for Systems Research and*
Dept. of Electrical and Computer Engineering
University of Maryland
College Park, MD 20742, USA

Abstract

This paper presents a Lie group setting for the problem of control of formations, as a natural outcome of the analysis of a planar two-vehicle formation control law. The vehicle trajectories are described using planar Frenet-Serret equations of motion, which capture the evolution of both the vehicle position and orientation for unit-speed motion subject to curvature (steering) control. The set of all possible (relative) equilibria for arbitrary G-invariant curvature controls is described (where $G = SE(2)$ is a symmetry group for the control law). A generalization of the control law for n vehicles is presented, and the corresponding (relative) equilibria are characterized. Work is on-going to discover stability and convergence results for the n-vehicle problem. The practical motivation for this work is the problem of formation control for meter-scale UAVs; therefore, an implementation approach consistent with UAV payload constraints is also discussed.

Key words: Frenet-Serret equations, nonlinear stability, Lyapunov function, formation control, shape space

1 Introduction

As the technological development of meter-scale UAVs (unmanned aerial vehices) progresses, and the cost of such vehicles decreases, there is growing interest in applications for formations (or swarms) of these UAVs. These applications include surveillance, creating decoys, delivery of payloads (e.g., distributing ground-based sensor networks), and radar or communications jamming. Having human operators remotely control each UAV in a formation is impractical; therefore, coordinating the flight of multiple UAVs becomes a problem of automatic control. In ongoing work, we are examining a particular approach to this control problem, with the ultimate objective of producing a prototype system capable of meeting the size, weight, and power constraints associated with small UAV platforms.

An essential feature of the formation control problem for meter-scale UAVs is that "autonomy" (e.g., sensors and processing power for target recognition, obstacle avoidance, GPS and inertial navigation, and performance of sophisticated mission objectives) is severly limited by cost and payload constraints. Consequently, we identify a few specific objectives, and attempt to formulate and implement a control law to meet these basic objectives. These objectives are to avoid collisions between UAVs, maintain the cohesiveness of the formation, be robust to loss of individuals, and scale favorably for large swarms. The challenge is that the physics of sensing, actuation, and communication cannot be neatly separated from the problem of coordination and control. Rather than simply extra payload, the automatic control system for formation control becomes an integral part of vehicle design.

In section 2, we describe how an automatic control system for formation flying could be practically implemented. The basic idea involves providing a mechanism (based on radio-frequency pulses) by which each UAV can sense its range and relative orientation with respect to its neighbors. We consider *simple* rules for how each UAV changes its motion in response to these "sensor" measurements. In terms of implementation, the hardware required for the controller on-board each UAV can, by incorporating analog VLSI circuitry, fit on a single small printed-circuit board. The objective is to supply the collection of UAVs with a "default" formation-maintaining behavior in such a way that the formation (as an entity) can be easily controlled, e.g., by modifying parameters, adding exogenous inputs, or switching among various "default" behaviors.

Models of the individual vehicles are based on the planar Frenet-Serret equations of motion (discussed in section 3), which describe how vehicle trajectories evolve under curvature (steering) control, subject to a unit-speed assumption [1]. While our interest is primarily in formation control for small UAVs, this approach to modeling and control could also be applicable to formations or

swarms of ground vehicles or underwater vehicles, and may also be a useful starting point for understanding certain features of biological swarming or schooling behavior.

This paper presents a Lie group setting for the problem of control of formations. The setting emerges naturally from the analysis of basic cases and concomitant physical contraints on the controls. (A modern reference for control systems on Lie groups is Jurdjevic [2].)

The primary analytical result we present (in section 4) is a global convergence result for a planar two-vehicle formation control law, proved using LaSalle's Invariance Principle [3]. A corresponding convergence result for a single vehicle responding to an omnidirectional beacon is also presented, and is used (in section 5) to help physically motivate the form of the two-vehicle control law, and to explain the relationship between the various sensor measurements and the quantities appearing in the control law. A generalization of the control law to n vehicles is presented in section 6, but a stability analysis is the subject of on-going work, and will be presented in a future paper.

The two-vehicle control law has an evident Lie-group structure, and this structure is exploited (in section 7) to determine the set of all possible (relative) equilibria for arbitrary G-invariant curvature controls, where $G = SE(2)$ is the symmetry group for the control law. Ideas of "shape control" on Lie groups arise in a natural way for this problem [4–6]. The equilibrium analysis is also generalized to the n-vehicle problem. Finally, in section 8, we discuss directions for future research.

The use of curvature controls can be given the mechanical interpretation of steering unit-mass, unit-charge particles by magnetic fields (and hence by forces derived from *vector* potentials). For a discussion of the general theory of such controls, see [7]. This is in contrast with other current approaches to formation control that are based on scalar potentials [8]. Furthermore, our emphasis on the Lie group structure of the control laws distinguishes our work from an established physics literature in the area of large collections of interacting particles subject to local interaction laws, and giving rise to pattern-forming systems, spatially localized coherent structures (e.g., flocks), and phase transitions (e.g., from disorder to order); see, for instance, [9–11].
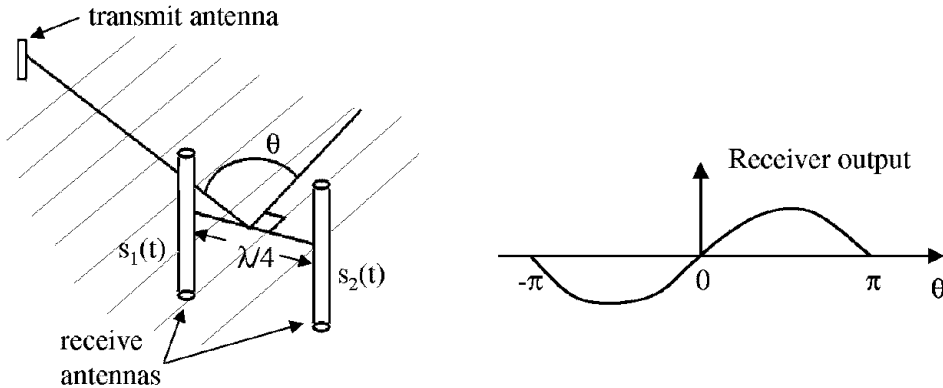
Fig. 1. A pair of receive antennas separated by a quarter-wavelength, and the sinusoidal function of angle-of-arrival which it can measure.

2 Formation control system implementation

2.1 Angle-of-arrival and range sensing

Consider the planar formation control problem: i.e., assume that there as a common plane of motion for the UAVs (and that this plane of motion does not change with time). Suppose that an RF (radio-frequency) transmit antenna, as well as a pair of receive antennas, are located in (and oriented perpendicular to) the plane of motion. (Neglect the mutual impedance of the receive antennas). If the receive antennas are spaced a quarter-wavelength apart, then by appropriate quadrature phase shifting, correlation (i.e., multiplication), and low-pass filtering, a sinusoidal function of the angle of arrival can be measured (see figure 1). The range, or distance between the transmitter and receiver, can also be measured (since it is inversely related to the received signal power).

If two pairs of receive antennas are used, oriented perpendicular to each other as shown in figure 2, then the direction of arrival of the received RF signal can be unambiguously determined. (Although dipole antennas are shown in figure 2, the actual antenna design would need to take into account aircraft aerodynamics and possible parasitic antenna elements. Noise, interference, and multipath are also important electromagnetics issues, but are also beyond the scope of this paper.) As figure 2 suggests, the antenna separation and hence the transmission frequency are related to the UAV dimensions.

It turns out that more information besides simply range and direction-of-arrival is useful for formation control. Specifically, we would also like to sense the relative orientation between the transmitting and receiving UAV. This extra information can be sensed if all four antennas shown in figure 2 participate in transmitting as well as receiving. Each pair of antennas, considered
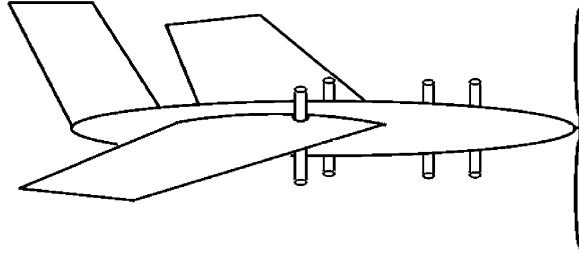
Fig. 2. Two pairs of receive antennas oriented perpendicularly on a UAV.

as a transmitting antenna array, has a cardioid antenna pattern if driven with single-tone pulses which are in phase-quadrature (figure 3(a)). Reversing the signals to the two antennas spatially reorients the cardioid antenna pattern by 180 degrees (figure 3(b)). If two quadrature signals at nearby but different frequencies are fed to the antennas simultaneously, but with the proper phase relationship so that the cardioid antenna patterns have their peaks in opposite directions, then by differencing the (normalized) amplitudes (i.e., power measurements) of the received pulses, a remote UAV can extract information about the orientation of the transmitting UAV relative to the baseline between the two UAVs (figure 3(c)). If both pairs of half-wave dipole antennas are driven (with four nearby but different frequencies) in this way (figure 3(d)), then the remote UAV will have enough sensor information to unambiguously measure the mutual orientation of the two UAVs.

After presenting and analyzing a specific control law in sections 3 and 4, we will explicitly show (in section 5) how the various quantities in the control law correspond to relative orientation and range measurements of the type just described.

2.2 Pulsed communication scheme

In the previous subsection, we discussed how RF signals and appropriate antenna configurations can permit each UAV to sense range and orientation relative to the other UAVs. One approach for reducing power consumption while keeping the system complexity low is to transmit RF pulses, as shown in figure 4, rather than continuous-wave signals. The UAVs take turns transmitting pulses (or bursts), and except when transmitting, each UAV listens to the others. (Of course, some scheme is required to organize the pulsed communication and prevent simultaneous transmissions, but these details are beyond the scope of this paper.) The PRI (pulse repetition interval), pulse width, and power consumption depend on the frequency, the number of UAVs, and the required UAV control signal update rate. Thus, the communication system depends intimately upon vehicle characteristics, such as its dimensions and dynamical constraints.
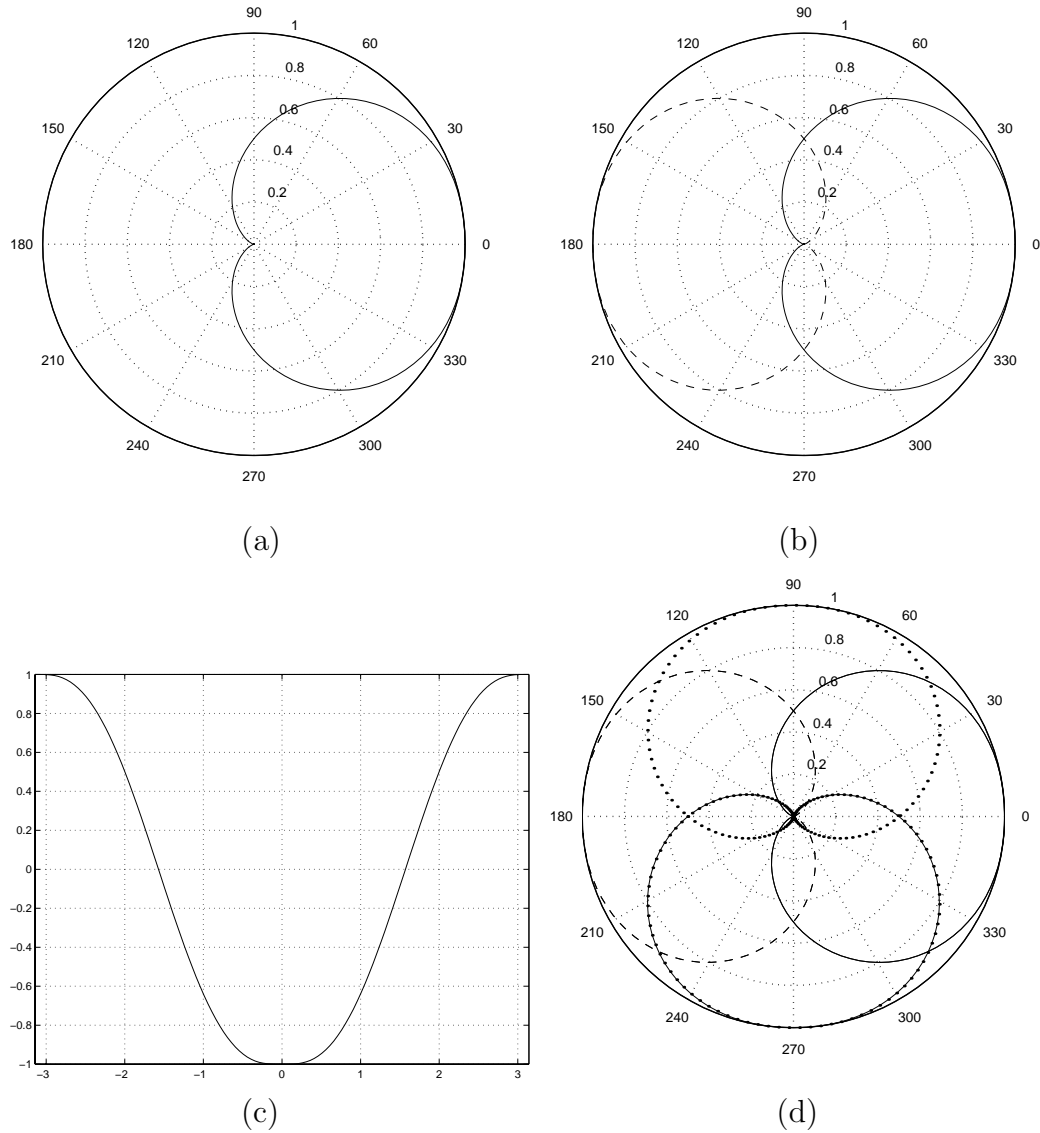
Fig. 3. Using two pairs of antennas for extracting relative orientation information: (a) cardioid antenna pattern for a single pair of antennas and a single tone; (b) cardioid antenna patterns for a single pair of antennas and two tones at different frequencies; (c) difference in received signal power as a function of angle between the transmitting UAV and the baseline; and (d) cardioid antenna patterns for two pairs of antennas and tones at four different frequencies.

Using this type of pulsed communication system avoids the need for a data communication network for formation control. (Of course, if a data communication network were available, the UAVs could determine their own positions and orientations using GPS, and then exchange the information with each other over the data communication network.) The main drawback with using a data communication network is the interplay between the communications and the control aspects of the resulting communicating networked control system. (Note, for example, that as the UAVs move, the network topology may
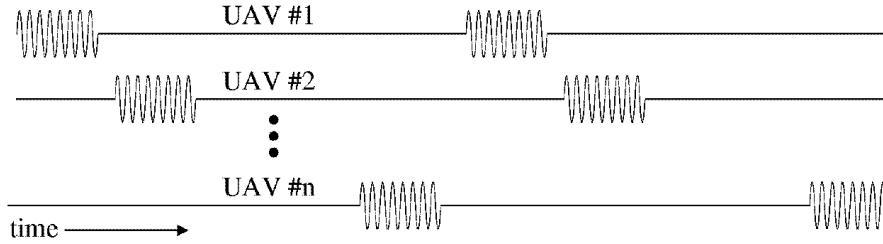
6

Fig. 4. Pulsed communication system: the UAVs take turns transmitting pulses, and except when transmitting, each UAV listens to the others.

change.) Using a data communication network for control requires careful attention to communication protocols, can introduce problems of scalability for large formations, and can be extremely difficult to analyze. An additional benefit of the pulsed communication scheme is reduced reliance on GPS.

The pulsed communication scheme uses time-division-multiplexing to share the communications bandwidth among multiple transmitters. One reason for chosing this scheme is to facilitate prototyping. Of course, other channel-sharing techniques like CDMA (code division multiple access) might ultimately be useful for improving stealth capability and reducing succeptibility to jamming.

2.3 Transceiver/controller block diagram

Figure 5 shows the block diagram for a transceiver/controller capable of implementing the control systems we consider based on the pulsed communication scheme described in the previous subsection. The four antennas represent the two pairs of antennas in figure 2. When the UAV is listening, the antenna signals pass through the transmit/receive switches to the low-noise-amplifiers and bandpass filters. Next, the signals arrive at an analog processor, which produces the various range and orientation measurements described above, and combines them into a single steering control increment each time an RF pulse is received. This steering control increment is then digitized and sent to a digital processor. The analog processor also has an output signal (an activity indicator) to tell the digital processor whether its steering control increment represents valid data. The digital processor accumulates the steering control increments over a full period during which each other UAV is transmitting, and then updates a steering control signal that it sends to the UAV autopilot. The digital processor is also responsible for controlling when the UAV transmits, and when it listens. During the transmitting phase, the required quadrature oscillator signals (which can be generated by the analog processor) are amplified, and sent to the antennas through the transmit/receive switches. The digital processor can also have a control line to the analog processor, so
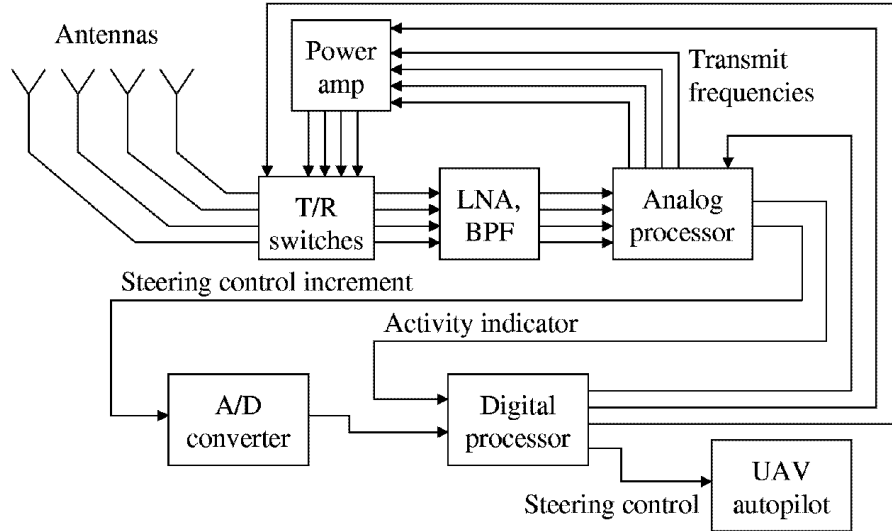
7

Fig. 5. Transceiver/controller block diagram for UAV control based on pulsed communication.

that, e.g., control law parameters can be varied on the fly.

The digital processor is thus involved with organizing the pulsed communication, interfacing with the autopilot, and could also potentially filter (or reject corrupted data from) the analog processor signal. Although not indicated in figure 5, the digital processor can also interface with a higher-level control system on board the UAV, which may communicate with the ground or other UAVs using a data communication network. Such data communication could be used to control the formation as a whole, with the basic formation-maintaining function being performed by the pulsed communication system and block diagram of figure 5.

The key feature of figure 5 is that (apart from the antennas and autopilot) the entire system could potentially fit on a single printed circuit board small enough to fit into a meter-scale UAV, provided the analog processor is implemented using analog VLSI technology. There are some similarities between the analog processor in figure 5 and the analog CMOS continuous wavelet transform circuits developed at the Naval Research Laboratory [12]. There is thus a feasibility demonstration of some of the required subcomponents of an analog VLSI processor for the UAV formation control application.

The possibility of producing a practical *prototype* formation controller for meter-scale UAVs is precisely what motivates the modeling and analysis presented in the following sections (although building such a prototype controller would still be a project in its own right). However, the modeling and analysis might be useful for other formation control problems as well (e.g., for ground or underwater vehicles). As long as the required range and orientation quantities can be measured and communicated to the appropriate vehicles,
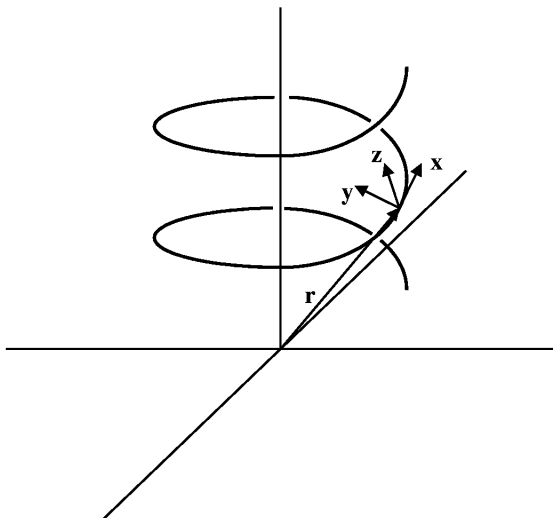
Fig. 6. UAV trajectory illustrating definitions of $\mathbf{x}$, $\mathbf{y}$, $\mathbf{z}$, and $\mathbf{r}$.

the control laws we present may be useful.

3 Modeling UAV formations

Each UAV trajectory is given a kinematic description using (a variant of) the well-known Frenet-Serret equations of motion, where at each point along the trajectory one attaches a moving frame (of unit tangent, normal, and binormal vectors) [1]. For a single UAV, the evolution equation we consider is

$$
\begin{aligned}
\dot{\mathbf{r}} &= \mathbf{x} \\
\dot{\mathbf{x}} &= \mathbf{y}u - \mathbf{z}v \\
\dot{\mathbf{y}} &= -\mathbf{x}u + \mathbf{z}w \\
\dot{\mathbf{z}} &= \mathbf{x}v - \mathbf{y}w,
\end{aligned}
\tag{1}
$$

where $\mathbf{r}$ is the position of the UAV; $\mathbf{x}$, $\mathbf{y}$, and $\mathbf{z}$ are orthonormal vectors specifying the orientation of the UAV; and u, v, and w are scalar control inputs (any two of which are sufficient to specify the motion). As shown in figure 6, $\mathbf{x}$ specifies the unit tangent vector to the UAV trajectory, $\mathbf{y}$ is normal to the trajectory, and $\mathbf{z}$ (the binormal) completes the orthonormal frame.

Using a kinematic description of the motion allows us to consider the formation control laws independently of the dynamics of individual vehicles. The formation control laws we consider would be implemented as simple commands supplied to each UAV's on-board autopilot, which has already been designed to account for the vehicle dynamics. Although optimal energy use is an im-

portant criterion for UAVs, our philosophy is to try to provide near-optimal energy use in the UAVs by studying optimality criteria within the framework of our kinematic models. At this stage in our investigations, however, we are simply trying to demonstrate models with basic formation-maintaining behaviour.

Note that the Frenet-Serret frame for the UAV corresponds to the trajectory followed by the UAV, not to the orientation of the UAV itself. For example, an aircraft would normally change direction by banking (rather than by yawing, as would be required if the Frenet-Serret frame described its orientation). For purposes of the idealized control laws we present, the Frenet-Serret frame is the one that applies. (The UAV-fixed frame could play an important role, however, in the control system implementation based on pairs of antennas and pulsed communication, an issue which merits further investigation.)

To reduce from a three-dimensional Frenet-Serret model to a planar model, we simply set the controls v and w to zero in equation (1), which eliminates the dynamical equation for $\mathbf{z}$. In this case, it is assumed that each UAV has some alternative method of determing the appropriate altitude. We allow for the possibility that the UAVs are flying at the same altitude, so that collision avoidance is a consideration.

4   Planar control law analysis

4.1   Control law for a pair of vehicles

Consider two vehicles modeled as point particles moving in the plane. Figure 7(a) illustrates the trajectories of the two vehicles, and their respective planar Frenet-Serret frames. The control law specifies the steering commands u_1 and u_2 for each vehicle. We present a convergence result for the system of two vehicles. In section 5 we discuss the physical interpretation and motivation for the control law.

Our model for the pair of vehicles and associated feedback control law is the following:

$$\dot{\mathbf{r}}_1 = \mathbf{x}_1, \qquad \dot{\mathbf{r}}_2 = \mathbf{x}_2,$$
$$\dot{\mathbf{x}}_1 = \mathbf{y}_1 u_1, \qquad \dot{\mathbf{x}}_2 = \mathbf{y}_2 u_2,$$
$$\dot{\mathbf{y}}_1 = -\mathbf{x}_1 u_1, \qquad \dot{\mathbf{y}}_2 = -\mathbf{x}_2 u_2,$$
$$u_1 = -\eta(|\mathbf{r}|)\left(-\frac{\mathbf{r}}{|\mathbf{r}|}\cdot\mathbf{x}_1\right)\left(-\frac{\mathbf{r}}{|\mathbf{r}|}\cdot\mathbf{y}_1\right) - f\left(|\mathbf{r}|\right)\left(-\frac{\mathbf{r}}{|\mathbf{r}|}\cdot\mathbf{y}_1\right) + \mu(|\mathbf{r}|)\mathbf{x}_2\cdot\mathbf{y}_1,$$
$$u_2 = -\eta(|\mathbf{r}|)\left(\frac{\mathbf{r}}{|\mathbf{r}|}\cdot\mathbf{x}_2\right)\left(\frac{\mathbf{r}}{|\mathbf{r}|}\cdot\mathbf{y}_2\right) - f\left(|\mathbf{r}|\right)\left(\frac{\mathbf{r}}{|\mathbf{r}|}\cdot\mathbf{y}_2\right) + \mu(|\mathbf{r}|)\mathbf{x}_1\cdot\mathbf{y}_2, \quad (2)$$

where $\mathbf{r} = \mathbf{r}_2 - \mathbf{r}_1$, the functions $\eta(\cdot)$, $\mu(\cdot)$, and $f(\cdot)$ are Lipschitz continuous, and $f(\cdot)$ satisfies

$$\lim_{\rho\to 0} f(\rho) = -\infty,$$
$$\lim_{\rho\to\infty} \int_{\tilde{\rho}}^{\rho} f(\hat{\rho})d\hat{\rho} = \infty, \text{ for some } \tilde{\rho} > 0. \tag{3}$$

We further assume that $\eta(|\mathbf{r}|) > 0$ and $\mu(|\mathbf{r}|) > 0$ for all $|\mathbf{r}| \geq 0$.

Identifying (punctured) $\mathbb{R}^2$ with the (punctured) complex plane, we define

$$\mathbf{r} = \mathbf{r}_2 - \mathbf{r}_1 = |\mathbf{r}|i e^{i\psi},$$
$$\mathbf{x}_1 = e^{i\theta_1},$$
$$\mathbf{x}_2 = e^{i\theta_2},$$
$$\phi_1 = \theta_1 - \psi,$$
$$\phi_2 = \theta_2 - \psi, \tag{4}$$

where we note that $\psi + \frac{\pi}{2}$ is the argument (i.e., angle) of $\mathbf{r}$. We introduce the variable

$$\rho = |\mathbf{r}|, \tag{5}$$

and we observe that

$$\frac{\mathbf{r}}{|\mathbf{r}|}\cdot\mathbf{x}_1 = \mathrm{Re}\left\{ie^{i\psi}\left(e^{i\theta_1}\right)^*\right\} = \sin(\theta_1 - \psi) = \sin\phi_1,$$
$$\frac{\mathbf{r}}{|\mathbf{r}|}\cdot\mathbf{x}_2 = \sin\phi_2,$$
$$\frac{\mathbf{r}}{|\mathbf{r}|}\cdot\mathbf{y}_1 = \mathrm{Re}\left\{ie^{i\psi}\left(ie^{i\theta_1}\right)^*\right\} = \cos(\theta_1 - \psi) = \cos\phi_1$$
$$\frac{\mathbf{r}}{|\mathbf{r}|}\cdot\mathbf{y}_2 = \cos\phi_2. \tag{6}$$

Figure 7(b) illustrates the definitions of ρ, ϕ_1, and ϕ_2.

Using

$$\dot{\mathbf{r}} = ie^{i\psi}\frac{d}{dt}|\mathbf{r}| - |\mathbf{r}|e^{i\psi}\dot{\psi} = \mathbf{x}_2 - \mathbf{x}_1 = e^{i\theta_2} - e^{i\theta_1}, \tag{7}$$
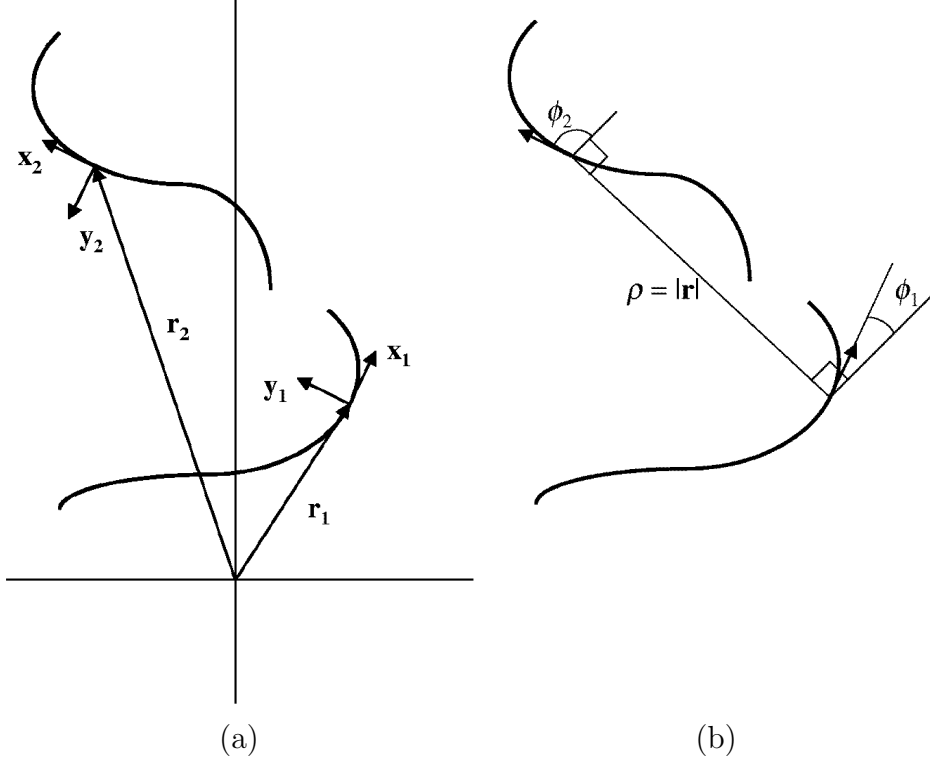
Fig. 7. Planar trajectories for two vehicles and their respective planar Frenet-Serret frames: (a) in $(\mathbf{r}_1, \mathbf{x}_1, \mathbf{y}_1), (\mathbf{r}_2, \mathbf{x}_2, \mathbf{y}_2)$ coordinates, and (b) in (ρ, ϕ_1, ϕ_2) coordinates.

we find that

$$
\begin{aligned}
\dot{\rho} &= \sin \phi_2 - \sin \phi_1, \\
\dot{\psi} &= -\frac{1}{\rho} \left(\cos \phi_2 - \cos \phi_1 \right).
\end{aligned}
\tag{8}
$$

We also have

$$
\begin{aligned}
\dot{\theta}_1 &= u_1 = -\eta(\rho) \sin \phi_1 \cos \phi_1 + f(\rho) \cos \phi_1 + \mu(\rho) \sin(\theta_2 - \theta_1), \\
\dot{\theta}_2 &= u_2 = -\eta(\rho) \sin \phi_2 \cos \phi_2 - f(\rho) \cos \phi_2 + \mu(\rho) \sin(\theta_1 - \theta_2).
\end{aligned}
\tag{9}
$$

We thus obtain the system

$$
\begin{aligned}
\dot{\rho} &= \sin \phi_2 - \sin \phi_1, \\
\dot{\phi}_1 &= -\eta(\rho) \sin \phi_1 \cos \phi_1 + f(\rho) \cos \phi_1 + \mu(\rho) \sin(\phi_2 - \phi_1) + \frac{1}{\rho} \left(\cos \phi_2 - \cos \phi_1 \right), \\
\dot{\phi}_2 &= -\eta(\rho) \sin \phi_2 \cos \phi_2 - f(\rho) \cos \phi_2 + \mu(\rho) \sin(\phi_1 - \phi_2) + \frac{1}{\rho} \left(\cos \phi_2 - \cos \phi_1 \right).
\end{aligned}
\tag{10}
$$

System (10) represents a reduction of the dynamics (2) by the symmetry group

12

$SE(2)$, which is made possible by the fact that the control law of equation (2) depends only on suitably defined shape variables, i.e., it is invariant under an action of the symmetry group SE(2). This point of view is made precise and further explored in section 7.

Consider the Lyapunov function candidate

$$V_{pair} = -\ln\left(\cos(\phi_2 - \phi_1) + 1\right) + h(\rho), \tag{11}$$

where $f(\rho) = dh/d\rho$. Differentiating V_{pair} with respect to time along (10) gives

$$
\begin{aligned}
\dot{V}_{pair} &= \frac{\sin(\phi_2 - \phi_1)}{\cos(\phi_2 - \phi_1) + 1}\left(\dot{\phi}_2 - \dot{\phi}_1\right) + f(\rho)\dot{\rho} \\
&= \frac{\sin(\phi_2 - \phi_1)}{\cos(\phi_2 - \phi_1) + 1}\Bigg[-\eta(\rho)\left(\sin\phi_2\cos\phi_2 - \sin\phi_1\cos\phi_1\right) + 2\mu(\rho)\sin(\phi_1 - \phi_2) \\
&\qquad\qquad\qquad\qquad\qquad\qquad\qquad\qquad\qquad -f(\rho)\left(\cos\phi_2 + \cos\phi_1\right)\Bigg] \\
&\quad + f(\rho)\left(\sin\phi_2 - \sin\phi_1\right) \\
&= \frac{-1}{\cos(\phi_2 - \phi_1) + 1}\Bigg[\sin(\phi_2 - \phi_1)\left(2\mu(\rho)\sin(\phi_2 - \phi_1) + \frac{\eta(\rho)}{2}\left(\sin 2\phi_2 - \sin 2\phi_1\right)\right) \\
&\qquad\qquad\qquad\qquad\qquad +f(\rho)\sin(\phi_2 - \phi_1)(\cos\phi_2 + \cos\phi_1) \\
&\qquad\qquad\qquad\qquad\qquad -f(\rho)(\cos(\phi_2 - \phi_1) + 1)(\sin\phi_2 - \sin\phi_1)\Bigg] \\
&= \frac{-1}{\cos(\phi_2 - \phi_1) + 1}\Bigg[\sin(\phi_2 - \phi_1)\left(2\mu(\rho)\sin(\phi_2 - \phi_1) + \frac{\eta(\rho)}{2}\left(\sin 2\phi_2 - \sin 2\phi_1\right)\right)\Bigg],
\end{aligned}
\tag{12}
$$

where we have used the identity (see Appendix A)

$$\sin(\phi_2 - \phi_1)(\cos\phi_2 + \cos\phi_1) - (\cos(\phi_2 - \phi_1) + 1)(\sin\phi_2 - \sin\phi_1) = 0. \tag{13}$$

We also have the identity (see Appendix A)

$$
\begin{aligned}
\sin(\phi_2 - \phi_1)&\left(\sin(\phi_2 - \phi_1) + \frac{1}{2}(\sin 2\phi_2 - \sin 2\phi_1)\right) \\
&= \frac{1}{2}\left[(\cos\phi_1 + \cos\phi_2)^2(\sin\phi_1 - \sin\phi_2)^2 + \left(\sin^2\phi_1 - \sin^2\phi_2\right)^2\right]. \tag{14}
\end{aligned}
$$

Therefore, provided $2\mu(\rho) > \eta(\rho), \quad \forall\rho \geq 0$, it follows that $\dot{V}_{pair} \leq 0$, and $\dot{V}_{pair} = 0$ if and only if $\sin(\phi_2 - \phi_1) = 0$. We can use this calculation to prove a convergence result.

Proposition 1: Consider the system given by equation (10), evolving on $\mathbb{R} \times \mathbb{T}^2$, where $\mathbb{T}^2$ is the two-torus (i.e., $\phi_i + 2\pi$ is identified with ϕ_i, $i = 1, 2$). In addition, assume the following:

(1) $\eta(\rho)$, $\mu(\rho)$, and $f(\rho)$ are Lipschitz continuous on $(0, \infty)$;
(2) $f(\rho) = dh/d\rho$, so that $h(\rho)$ is continuously differentiable on $(0, \infty)$;
(3) $\lim_{\rho \to 0} h(\rho) = \infty$, $\lim_{\rho \to \infty} h(\rho) = \infty$, and $\exists \tilde{\rho}$ such that $h(\tilde{\rho}) = 0$;
(4) $\eta(\rho) > 0$, $\mu(\rho) > 0$, and $2\mu(\rho) > \eta(\rho)$, $\forall \rho \geq 0$.

Define the set $\Lambda = \left\{ (\rho, \phi_1, \phi_2) \middle| |\phi_1 - \phi_2| \neq \pi \text{ and } 0 < \rho < \infty \right\}$. Then any trajectory starting in Λ converges to the set of equilibrium points for system (10).

Proof: Observe that V_{pair} given by equation (11) is continuously differentiable on Λ. By assumption (2) and the form of V_{pair}, we conclude that V_{pair} is radially unbounded (i.e., $V_{pair} \to \infty$ as $|\phi_1 - \phi_2| \to \pi$, as $\rho \to 0$, or as $\rho \to \infty$). Therefore, for each trajectory starting in Λ there exists a compact sublevel set Ω of V_{pair} such that the trajectory remains in Ω for all future time. Then by LaSalle's Invariance Principle, the trajectory converges to the largest invariant set M of the set E of all points in Ω where $\dot{V}_{pair} = 0$ [3]. The set E in this case is the set of all points $(\rho, \phi_1, \phi_2) \in \Omega$ such that $\sin(\phi_1 - \phi_2) = 0$, i.e., such that $\phi_1 = \phi_2$ (since $\Omega \subset \Lambda$). At points in E, the dynamics may be expressed as

$$
\begin{aligned}
\dot{\rho} &= 0, \\
\dot{\phi}_1 &= -[\eta(\rho) \sin \phi_1 + f(\rho)] \cos \phi_1, \\
\dot{\phi}_2 &= -[\eta(\rho) \sin \phi_1 - f(\rho)] \cos \phi_1.
\end{aligned}
\tag{15}
$$

If $\phi_1 \neq \pm\pi/2$ and $f(\rho) \neq 0$, then the trajectory leaves E. The largest invariant set contained in E may thus be expressed as

$$
M = \left(\left\{ (\rho, \tfrac{\pi}{2}, \tfrac{\pi}{2}), \ \forall \rho \right\} \cup \left\{ (\rho, -\tfrac{\pi}{2}, -\tfrac{\pi}{2}), \ \forall \rho \right\} \cup \left\{ (\rho_e, 0, 0) \middle| f(\rho_e) = 0 \right\} \right) \cap \Omega,
\tag{16}
$$

which is simply the set of equilibria of the system (10) contained in Ω. $\square$

A physical interpretation of this convergence result (and the set M) is provided in subsection 5.4.

4.2 Control law for a single vehicle (and fixed beacon)

We now present a control law for a single vehicle based on its position and orientation relative to a "beacon" fixed at the origin, as illustrated in figure 8(a):

$$
\begin{aligned}
\dot{\mathbf{r}} &= \mathbf{x}, \\
\dot{\mathbf{x}} &= \mathbf{y}u, \\
\dot{\mathbf{y}} &= -\mathbf{x}u, \\
u &= -\eta(|\mathbf{r}|)\left(\frac{\mathbf{r}}{|\mathbf{r}|}\cdot\mathbf{x}\right)\left(\frac{\mathbf{r}}{|\mathbf{r}|}\cdot\mathbf{y}\right) - f(|\mathbf{r}|)\left(\frac{\mathbf{r}}{|\mathbf{r}|}\cdot\mathbf{y}\right).
\end{aligned}
\tag{17}
$$

Define

$$
\begin{aligned}
\mathbf{r} &= |\mathbf{r}|i e^{i\psi}, \\
\mathbf{x} &= e^{i\theta}, \\
\rho &= |\mathbf{r}|, \\
\phi &= \theta - \psi.
\end{aligned}
\tag{18}
$$

(The variables ρ and ϕ are illustrated in figure 8(b).) Then we obtain, analogously to system (10),

$$
\begin{aligned}
\dot{\rho} &= \sin\phi, \\
\dot{\phi} &= -\eta(\rho)\sin\phi\cos\phi - \left(f(\rho) - \frac{1}{\rho}\right)\cos\phi.
\end{aligned}
\tag{19}
$$

Consider the Lyapunov function candidate

$$
V_{single} = -\ln(\cos\phi) + h(\rho),
\tag{20}
$$

defined on the set

$$
\Lambda_{single} = \left\{ (\rho,\phi) \,\middle|\, \rho > 0, \ -\frac{\pi}{2} < \phi < \frac{\pi}{2} \right\},
\tag{21}
$$

and where $f(\rho) - 1/\rho = dh/d\rho$. We then compute

$$
\begin{aligned}
\dot{V}_{single} &= \left(\frac{\sin\phi}{\cos\phi}\right)\dot{\phi} + \left(f(\rho) - \frac{1}{\rho}\right)\dot{\rho} \\
&= \frac{\sin\phi}{\cos\phi}\left[-\eta(\rho)\sin\phi\cos\phi - \left(f(\rho) - \frac{1}{\rho}\right)\cos\phi\right] + \left(f(\rho) - \frac{1}{\rho}\right)\sin\phi \\
&= -\eta(\rho)\sin^2\phi.
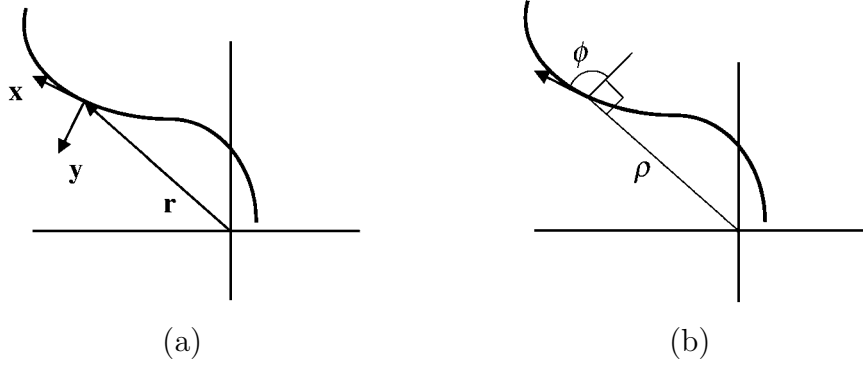\end{aligned}
\tag{22}
$$

15

Fig. 8. Planar trajectory and Frenet-Serret frame for a single vehicle responding to a fixed beacon: (a) in $(\mathbf{r}, \mathbf{x}, \mathbf{y})$ coordinates, and (b) in (ρ, ϕ) coordinates.

Based on this calculation, we can prove a convergence result.

Proposition 2: Consider the system given by equation (19), evolving on $\mathbb{R} \times \mathbb{T}^1$, where $\mathbb{T}^1$ is the one-torus (i.e., $\phi + 2\pi$ is identified with ϕ). In addition, assume the following:

(1) $\eta(\rho)$ and $f(\rho)$ are Lipschitz continuous on $(0, \infty)$;
(2) $f(\rho) = dh/d\rho$, so that $h(\rho)$ is continuously differentiable on $(0, \infty)$;
(3) $\lim_{\rho \to 0} h(\rho) = \infty$, $\lim_{\rho \to \infty} h(\rho) = \infty$ and $\exists \tilde{\rho}$ such that $h(\tilde{\rho}) = 0$;
(4) $\eta(\rho) > 0, \quad \forall \rho \geq 0$.

Let Λ_{single} be defined by equation (21). Then any trajectory starting in Λ_{single} converges to the set of equilibrium points for system (10), i.e., the set

$$\Gamma_e = \left\{ (\rho, \phi) \,\middle|\, \left(f(\rho) - \frac{1}{\rho} \right) = 0, \quad \phi = 0 \right\}. \tag{23}$$

Proof: Observe that V_{single} given by equation (20) is continuously differentiable on Λ_{single}. By assumption (2) and the form of V_{single}, we conclude that V_{single} is radially unbounded (i.e., $V_{single} \to \infty$ as $|\phi| \to \frac{\pi}{2}$, as $\rho \to 0$, or as $\rho \to \infty$). Therefore, for each trajectory starting in Λ_{single} there exists a compact sublevel set Ω of V_{single} such that the trajectory remains in Ω for all future time. Then by LaSalle's Invariance Principle, the trajectory converges to the largest invariant set M of the set E of all points in Ω where $\dot{V}_{single} = 0$ [3]. The set E in this case is the set of all points $(\rho, \phi) \in \Omega$ such that $\sin(\phi) = 0$, i.e., such that $\phi = 0$ (since $\Omega \subset \Lambda_{single}$). At points in E, the dynamics may be expressed as

$$\dot{\rho} = 0,$$
$$\dot{\phi} = -\left(f(\rho) - \frac{1}{\rho} \right). \tag{24}$$

16

If $\left(f(\rho) - \frac{1}{\rho}\right) \neq 0$, then the trajectory leaves E. The largest invariant set contained in E may thus be expressed as

$$M = \Gamma_e \cap \Omega, \tag{25}$$

which is simply the set of equilibria of the system (19) contained in Ω. $\square$

Remark: If the set Γ_e consists of isolated points, then **Proposition 2** implies that each trajectory starting in Λ_{single} converges to an equilibrium point. $\square$

Remark: A result analogous to **Proposition 2** holds for trajectories starting in

$$\Lambda_{single}^{alt} = \left\{ (\rho, \phi) \middle| \rho > 0, \ |\phi| > \frac{\pi}{2} \right\}. \tag{26}$$

Instead of V_{single} defined by equation (20), the Lyapunov function

$$V_{single}^{alt} = -\ln(-\cos \phi) + h(\rho) \tag{27}$$

is used. $\square$

5   Physical motivation for the planar control law

In this section we provide some physical motivation for the control law analyzed in the previous section, as well as a physical interpretation of the convergence result. The objective is primarily to suggest why this control law is the simplest that could reasonably be expected to perform well. (While the purpose of the previous section was to provide careful mathematical statements, here we adopt a more pragmatic approach for purposes of conveying physical intuition.)

5.1   Achieving a common orientation

In system (2), the term $\mu(|\mathbf{r}|)\mathbf{x}_2 \cdot \mathbf{y}_1$ in the equation for u_1, and the term $\mu(|\mathbf{r}|)\mathbf{x}_1 \cdot \mathbf{y}_2$ in the equation for u_2, can be easily interpreted as serving to drive the two vehicles to a common orientation. In fact, this approach generalizes for driving n vehicles to a common orientation. For $\mu > 0$ constant, consider the control law

$$\dot{\mathbf{r}}_k = \mathbf{x}_k,$$
$$\dot{\mathbf{x}}_k = \mathbf{y}_k u_k,$$
$$\dot{\mathbf{y}}_k = -\mathbf{x}_k u_k,$$
$$u_k = \mu \sum_{\substack{j \neq k}}^{n} \mathbf{x}_j \cdot \mathbf{y}_k, \tag{28}$$

for $k = 1, ..., n$. Observe that $\dot{\mathbf{r}}_k = \mathbf{x}_k$ decouples from the rest of equation (28).

Introducing complex notation, we define

$$\mathbf{x}_j = e^{i\theta_j}, \tag{29}$$

so that the dynamics can be written in θ_j coordinates as

$$\dot{\theta}_j = u_j = \mu \sum_{k \neq j} \operatorname{Re}\left\{ e^{i\theta_k} \left(i e^{i\theta_j} \right)^* \right\} = \mu \sum_{k \neq j} \sin(\theta_k - \theta_j). \tag{30}$$

It is well known that system (30) is a gradient system with respect to the energy function

$$V_{orient} = -\frac{\mu}{2} \sum_{j,k} \cos(\theta_k - \theta_j), \tag{31}$$

i.e.,

$$\dot{\theta}_j = -\frac{\partial V_{orient}}{\partial \theta_j}. \tag{32}$$

The control law (28) thus acts to reorient the vehicles so that they all head in the same direction. Furthermore, the heading direction for the formation is determined by an averaging-like process based on the initial orientations. While these are both laudable properties, there is a weakness to this control scheme, as it stands, for formation initiation: there is no control of the relative positions of the vehicles in the formation. We would like to augment this reorientation scheme with some approach for maintaining swarm cohesiveness, while avoiding collisions.

5.2 Achieving appropriate separation

To understand how an appropriate vehicle separation is maintained by system (2), it is helpful to first consider the single-vehicle system given by equation (17). Suppose for simplicity that there exists a single value $\rho_o > 0$ such that $(f(\rho_o) - 1/\rho_o) = 0$. Then under the assumptions of **Proposition 2**, for almost all initial conditions (i.e., provided $|\phi| \neq \frac{\pi}{2}$ initially), system (19) converges to one of two equilibrium points: either $(\rho_o, 0)$ or (ρ_o, π). The corresponding solutions for system (17) are circular orbits centered at the origin and with

radius ρ_o, and the two (relative) equilibria correspond to clockwise and counterclockwise orbits. The initial condition determines whether the orbit will be clockwise or counterclockwise, and the initial condition $|\phi| = \frac{\pi}{2}$ represents the vehicle heading directly toward (or directly away from) the origin.

Now consider the control law given by equation (2), but with $\mu \equiv 0$. Physically, this control law can be thought of as each vehicle using the control law given by equation (17), but with the other vehicle treated as the "beacon," rather than having a beacon fixed at the origin. (Due to space limitations, we do not provide any analytic statements for this system, so this discussion is informal.) This control law tends to appropriately separate the two vehicles; however, depending on initial conditions, they may either head off in the same direction, or else circle each other. Either of these behaviors is consistent with the beacon-circling behavior of a single vehicle governed by the control law of system (17).

We can thus understand physically the various control law terms in system (2) for a pair of vehicles as serving to achieve a common orientation and an appropriate separation. This physical interpretation is compatible with many biological swarming and schooling models, which tend to be characterized by (1) some mechanism for heading alignment, (2) switching between attraction or repulsion based on separation distance, and (3) greater responsiveness for small separations [13].

5.3 Angle quantities appearing in the control law

In the control law for a pair of vehicles, system (2), various dot products (representing sines and cosines of various angles) appear. The quantities $\left(\frac{\mathbf{r}}{|\mathbf{r}|} \cdot \mathbf{x}_i \right)$ and $\left(\frac{\mathbf{r}}{|\mathbf{r}|} \cdot \mathbf{y}_i \right)$ in the expression for u_i, $i = 1, 2$, indicate the orientation of the ith vehicle relative to the baseline between the two vehicles. These are the angle-of-arrival quantities that can be sensed from a single transmitted tone using the two pairs of antennas shown in figure 2. (Note that these are the only angle quantities required for the single vehicle control law, system (17).)

The quantities $\mathbf{x}_2 \cdot \mathbf{y}_1$ and $\mathbf{x}_1 \cdot \mathbf{y}_2$ can be expressed as

$$
\begin{aligned}
\mathbf{x}_2 \cdot \mathbf{y}_1 &= \left(\frac{\mathbf{r}}{|\mathbf{r}|} \cdot \mathbf{x}_2 \right) \left(\frac{\mathbf{r}}{|\mathbf{r}|} \cdot \mathbf{y}_1 \right) - \left(\frac{\mathbf{r}}{|\mathbf{r}|} \cdot \mathbf{y}_2 \right) \left(\frac{\mathbf{r}}{|\mathbf{r}|} \cdot \mathbf{x}_1 \right), \\
\mathbf{x}_1 \cdot \mathbf{y}_2 &= \left(\frac{\mathbf{r}}{|\mathbf{r}|} \cdot \mathbf{x}_1 \right) \left(\frac{\mathbf{r}}{|\mathbf{r}|} \cdot \mathbf{y}_2 \right) - \left(\frac{\mathbf{r}}{|\mathbf{r}|} \cdot \mathbf{y}_1 \right) \left(\frac{\mathbf{r}}{|\mathbf{r}|} \cdot \mathbf{x}_2 \right).
\end{aligned}
\tag{33}
$$

Thus, the relative orientation between the two vehicles can be determined from the relative orientations of each vehicle relative to the baseline between

them. For our implementation approach based on radio-frequency pulses, the orientation of a transmitting UAV relative to the baseline between the UAVs is sensed with the aid of the four cardioid transmit antenna patterns of figure 3(d).

5.4 Interpretation of the convergence result

Consider the control law for a pair of vehicles given by system (2). Suppose for simplicity that there exists a single value $\rho_o > 0$ such that $f(\rho_o) = 0$. Then the set of equilibria which system (10) can converge to consists of the isolated point $(\rho_o, 0, 0)$, the connected set $(\rho, \frac{\pi}{2}, \frac{\pi}{2})$, and the connected set $(\rho, -\frac{\pi}{2}, -\frac{\pi}{2})$. The isolated point $(\rho_o, 0, 0)$ is easily interpreted: both vehicles are heading in the same direction, perpendicular to the baseline between them, and separated by a distance ρ_o. This stable equilibrium minimizes V_{pair}. The other sets of equilibria correspond to the two vehicles heading in the same direction, one leading the other by a distance ρ (with the two sets distinguished by which vehicle is in the lead). These equilibria appear to be unstable.

The requirements on $f(\cdot)$ for **Proposition 1** to hold, namely

$$f(\rho) \text{ is (Lipschitz) continuous on } (0, \infty),$$

$$f(\rho) = \frac{dh}{d\rho}, \text{ with } h(\tilde{\rho}) = 0,$$

$$\lim_{\rho \to \infty} h(\rho) = \lim_{\rho \to \infty} \int_{\tilde{\rho}}^{\rho} f(\hat{\rho})d\hat{\rho} = \infty, \tag{34}$$

$$\lim_{\rho \to 0} h(\rho) = \lim_{\rho \to 0} \int_{\tilde{\rho}}^{\rho} f(\hat{\rho})d\hat{\rho} = \infty, \tag{35}$$

have some practical implications. For example, if $f(\rho) \approx \frac{1}{\rho}$ as $\rho \to \infty$, then equation (34) holds; however, if $f(\rho) \approx \frac{1}{\rho^2}$ as $\rho \to \infty$, then it does not. If $f(\rho)$ is derived from a physical measurement of received signal power from another UAV, then it would be natural for $f(\rho) \approx \frac{1}{\rho^2}$ as $\rho \to \infty$. This means our *model* of the physical system, for which **Proposition 1** holds, can only be valid provided the distance between the UAVs is not too large.

Equation (35) implies $f(\rho) \to -\infty$ as $\rho \to 0$. Physically, this suggests that the steering control for the vehicles can become infinite if the separation between the vehicles is small. Thus, our model of the system is only valid provided the vehicles remain sufficiently far apart. Although our model can only be valid for a certain range of distances between the vehicles, from **Proposition 1** we know that for our model, trajectories never leave sublevel sets of V_{pair}. Thus, as long as the two vehicles satisfy initial conditions within a sublevel set of

V_{pair}, throughout which the model agrees with the physical system, then the conclusion of **Proposition 1** remains valid.

6   A generalization of the planar control law to n vehicles

The control system given by equation (2) can be generalized to n vehicles as follows:

$$
\begin{aligned}
\dot{\mathbf{r}}_k &= \mathbf{x}_k, \\
\dot{\mathbf{x}}_k &= \mathbf{y}_k u_k, \\
\dot{\mathbf{y}}_k &= -\mathbf{x}_k u_k,
\end{aligned}
\tag{36}
$$

with

$$
u_k = \sum_{j \neq k} \left[-\eta \left(\frac{\mathbf{r}_{jk}}{|\mathbf{r}_{jk}|} \cdot \mathbf{x}_k \right) \left(\frac{\mathbf{r}_{jk}}{|\mathbf{r}_{jk}|} \cdot \mathbf{y}_k \right) - f(|\mathbf{r}_{jk}|) \left(\frac{\mathbf{r}_{jk}}{|\mathbf{r}_{jk}|} \cdot \mathbf{y}_k \right) + \mu \mathbf{x}_j \cdot \mathbf{y}_k \right], \tag{37}
$$

where $\mathbf{r}_{jk} = \mathbf{r}_k - \mathbf{r}_j$. One possible choice for $f(\cdot)$ is

$$
f(|\mathbf{r}_{jk}|) = \alpha \left[1 - \left(\frac{r_o}{|\mathbf{r}_{jk}|} \right)^2 \right], \tag{38}
$$

and μ, η, and α could also be functions of inter-vehicle distance. Observe that each vehicle trajectory evolves with its own planar Frenet-Serret equation, and that the control is simply a sum of terms analogous to those present in system (2).

A generalization of the energy function V_{pair} that might play a role in analyzing the convergence of this system is

$$
V_n = \sum_{k=1}^{n} \sum_{j<k} w_{jk} \left[-\ln\left(\cos(\theta_k - \theta_j) + 1 \right) + h(\rho_{jk}) \right], \tag{39}
$$

where the w_{jk} are positive weights (or weighting functions). We have not yet proved a convergence result for the n-vehicle system. However, simulation results, combined with **Proposition 1**, suggests that it may be possible to prove some sort of convergence result for the n-vehicle system.

Figure 9 shows the formation-initializing behavior for three different sets of random initial conditions. Observe that the ultimate heading direction for the formation is initial-condition dependent. Also, observe that the relative positions of the vehicles within the formation is somewhat irregular, although the spacings between neighbors are roughly consistent. It appears from the
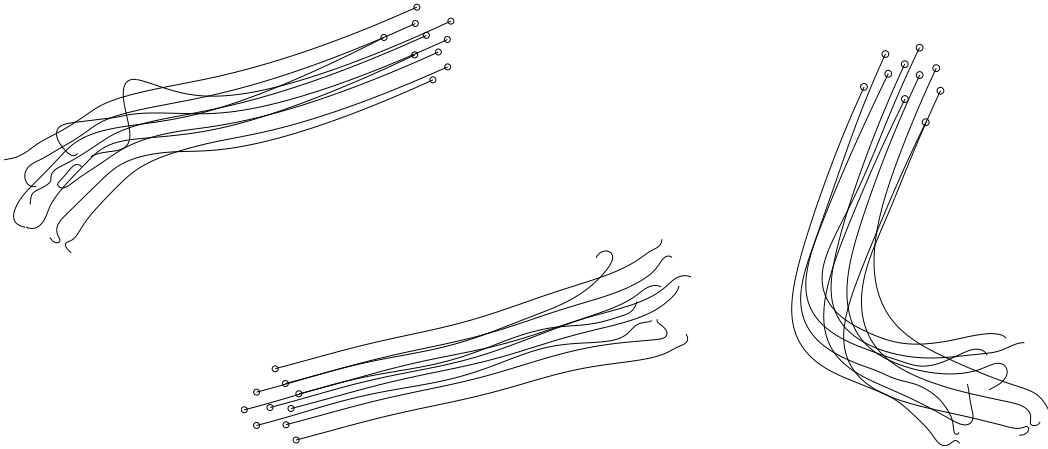
Fig. 9. Formation initialization for ten vehicles with three different sets of random initial conditions (in equations (36) and (37), $\eta = \mu = \alpha = \text{constant} = 0.02$).

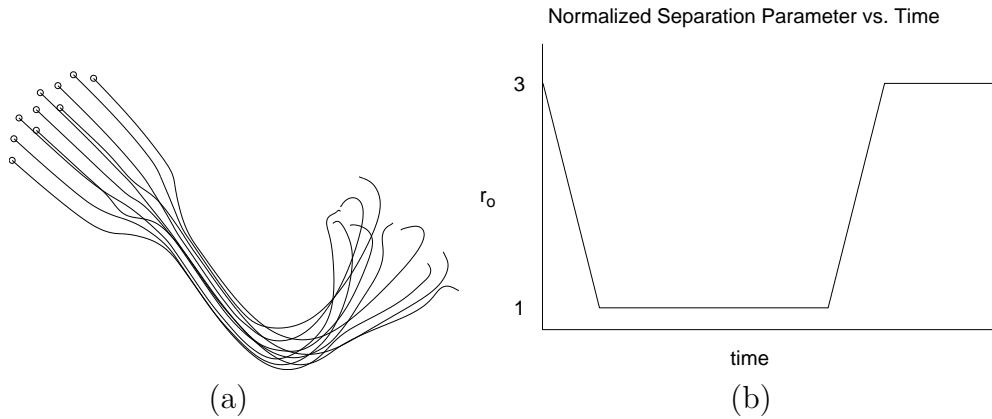Normalized Separation Parameter vs. Time

(a) (b)

Fig. 10. Formation flying for ten vehicles as the separation parameter is varied: (a) the vehicle trajectories, and (b) a semilog plot of the normalized separation parameter vs. time (where the time axis is linear).

simulation results that the control scheme given by equations (36) and (37) does indeed avoid collisions and maintain swarm cohesiveness.

Figure 10(a) illustrates how a single parameter, common to all the vehicles, can be varied to produce a global change in the formation. For this simulation, the length scale parameter (or separation parameter) α in equation (38) is varied with time as shown in figure 10(b). As α is decreased, the formation becomes more tight, and as α is increased, the separation between the vehicles increases.

Figure 11 illustrates "leader-following" behavior. The leader, i.e., the vehicle represented by the dashed path, follows a prescribed steering program, and is unaffected by the other vehicles. However, the other vehicles are influenced both by the leader and by each other. (Results are shown for two different
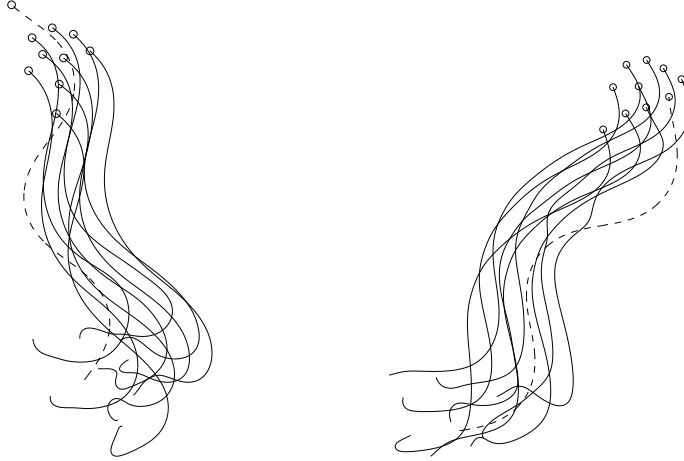
22

Fig. 11. Formation initialization for ten vehicles, one of which (dashed) follows a prescribed steering program unaffected by the other vehicles (for two different sets of random initial conditions).

sets of random initial conditions.) The influence of the leader on the formation behavior is evident; however, the leader need not be physically in front of the other vehicles. Indeed, this is by no means the only approach for generating leader-following behavior; nor is it necessarily the best approach. However, it clearly illustrates the possibility of allowing the control law of equations (36) and (37) to maintain the basic formation, while some additional control action guides the formation as a whole.

7 Lie group formulation and relative equilibria

7.1 Two-vehicle problem

There is a natural Lie group structure evident in system (2). In this subsection, we discuss how the formation control problem for two vehicles can be formulated as a "shape-control" problem in the Lie group setting [4–6]. We can consider the dynamics of system (2) as evolving on a (collision-free) configuration submanifold $M_{config} \subset G \times G$, where $G = SE(2)$ is the special Euclidean group in the plane. Specifically, if $g_1, g_2 \in G$ are represented as

$$g_1 = \begin{bmatrix} \mathbf{x}_1 & \mathbf{y}_1 & \mathbf{r}_1 \\ & & \\ 0 & 0 & 1 \end{bmatrix}, \quad g_2 = \begin{bmatrix} \mathbf{x}_2 & \mathbf{y}_2 & \mathbf{r}_2 \\ & & \\ 0 & 0 & 1 \end{bmatrix}, \quad (40)$$

23

then

$$M_{config} = \left\{ (g_1, g_2) \in G \times G \mid \mathbf{r}_1 \neq \mathbf{r}_2 \right\}. \tag{41}$$

(From **Proposition 1**, we can conclude that for initial conditions in M_{config}, the dynamics evolve in M_{config} for all future time, provided the controls given by equation (2) are used. However, for purposes of this section, we are primarily interested in identifying relative equilibria without restriction to a particular control law.) We can express the dynamics given by equation (2) as

$$\begin{aligned}
\dot{g}_1 &= g_1 \xi_1 = g_1 (A_0 + A_1 u_1), \\
\dot{g}_2 &= g_2 \xi_2 = g_2 (A_0 + A_1 u_2),
\end{aligned} \tag{42}$$

where $\xi_1, \xi_2 \in \mathfrak{g} =$ the Lie algebra of G, and the matrices A_0 and A_1 (which generate $\mathfrak{g}$ under Lie bracketing) are given by

$$A_0 = \begin{bmatrix} 0 & 0 & 1 \\ 0 & 0 & 0 \\ 0 & 0 & 0 \end{bmatrix}, \quad A_1 = \begin{bmatrix} 0 & -1 & 0 \\ 1 & 0 & 0 \\ 0 & 0 & 0 \end{bmatrix}. \tag{43}$$

We define

$$g = g_1^{-1} g_2, \tag{44}$$

and observe that

$$g = \begin{bmatrix} \mathbf{x}_1^T & -\mathbf{r}_1 \cdot \mathbf{x}_1 \\ \mathbf{y}_1^T & -\mathbf{r}_1 \cdot \mathbf{y}_1 \\ 0 \quad 0 & 1 \end{bmatrix} \begin{bmatrix} \mathbf{x}_2 & \mathbf{y}_2 & \mathbf{r}_2 \\ & & \\ 0 & 0 & 1 \end{bmatrix} = \begin{bmatrix} \mathbf{x}_1 \cdot \mathbf{x}_2 & \mathbf{x}_1 \cdot \mathbf{y}_2 & (\mathbf{r}_2 - \mathbf{r}_1) \cdot \mathbf{x}_1 \\ \mathbf{y}_1 \cdot \mathbf{x}_2 & \mathbf{y}_1 \cdot \mathbf{y}_2 & (\mathbf{r}_2 - \mathbf{r}_1) \cdot \mathbf{y}_1 \\ 0 & 0 & 1 \end{bmatrix}. \tag{45}$$

Similarly,

$$g^{-1} = g_2^{-1} g_1 = \begin{bmatrix} \mathbf{x}_1 \cdot \mathbf{x}_2 & \mathbf{x}_2 \cdot \mathbf{y}_1 & -(\mathbf{r}_2 - \mathbf{r}_1) \cdot \mathbf{x}_2 \\ \mathbf{y}_2 \cdot \mathbf{x}_1 & \mathbf{y}_1 \cdot \mathbf{y}_2 & -(\mathbf{r}_2 - \mathbf{r}_1) \cdot \mathbf{y}_2 \\ 0 & 0 & 1 \end{bmatrix}. \tag{46}$$

Let g_{ij} denote the elements of the matrix g, let g^{ij} denote the elements of the matrix g^{-1}, and let

$$r = \sqrt{g_{13}^2 + g_{23}^2} = \sqrt{(g^{13})^2 + (g^{23})^2}. \tag{47}$$

We have the following relationships among the g_{ij} and g^{ij}:

$$g_{11} = g_{22} = g^{11} = g^{22},$$
$$g_{12} = -g_{21} = g^{21} = -g^{12}, \tag{48}$$

and

$$g_{11}^2 + g_{12}^2 = 1. \tag{49}$$

Remark: We can express u_1 and u_2 as defined by equation (2) as

$$u_1(g) = -\eta(r) \left(\frac{g_{13}g_{23}}{r^2} \right) + f(r) \left(\frac{g_{23}}{r} \right) + \mu(r)g_{21},$$
$$u_2(g) = -\eta(r) \left(\frac{g^{13}g^{23}}{r^2} \right) + f(r) \left(\frac{g^{23}}{r} \right) + \mu(r)g^{21}. \tag{50}$$

Equations (42), (44), and (50) are sufficient to conclude that the closed-loop dynamics are G-invariant. Although we do not require the specific control law given by equation (50) for the (relative) equilibrium analysis presented in this subsection, we do assume that the control law is G-invariant, in addition to ensuring that the dynamics evolve in the collision-free submanifold. $\square$

Now,

$$\begin{aligned}
\dot{g} &= -g_1^{-1}\dot{g}_1 g_1^{-1} g_2 + g_1^{-1}\dot{g}_2 \\
&= -g_1^{-1}g_1\xi_1 g + g_1^{-1}g_2\xi_2 \\
&= -\xi_1 g + g\xi_2 \\
&= g(\xi_2 - g^{-1}\xi_1 g) \\
&= g(\xi_2 - \mathrm{Ad}_{g^{-1}}\xi_1) \\
&= g\xi, \tag{51}
\end{aligned}$$

where $\xi = \xi_2 - \mathrm{Ad}_{g^{-1}}\xi_1 \in \mathfrak{g}$. If the feedback controls depend only on the *shape variable* g, then $\xi = \xi(g)$ and (51) evolves on the shape space M_{config}/G.

We refer to (51) as the reduced dynamics. Equilibria of the reduced dynamics correspond to relative equilibria of the full dynamics in M_{config}. The equilibria g_e of the reduced dynamics are given by setting

$$\xi(g_e) = \xi_2(g_e) - g_e^{-1}\xi_1(g_e)g_e = 0. \tag{52}$$

Equation (52) is equivalent to

$$g_e\xi_2(g_e) = \xi_1(g_e)g_e, \tag{53}$$

which (dropping the "e" subscript) becomes

$$
\begin{bmatrix} g_{11} & g_{12} & g_{13} \\ -g_{12} & g_{11} & g_{23} \\ 0 & 0 & 1 \end{bmatrix} \begin{bmatrix} 0 & -u_2 & 1 \\ u_2 & 0 & 0 \\ 0 & 0 & 0 \end{bmatrix} = \begin{bmatrix} 0 & -u_1 & 1 \\ u_1 & 0 & 0 \\ 0 & 0 & 0 \end{bmatrix} \begin{bmatrix} g_{11} & g_{12} & g_{13} \\ -g_{12} & g_{11} & g_{23} \\ 0 & 0 & 1 \end{bmatrix}
$$

$$
\begin{bmatrix} g_{12}u_2 & -g_{11}u_2 & g_{11} \\ g_{11}u_2 & g_{12}u_2 & -g_{12} \\ 0 & 0 & 0 \end{bmatrix} = \begin{bmatrix} g_{12}u_1 & -g_{11}u_1 & 1-g_{23}u_1 \\ g_{11}u_1 & g_{12}u_1 & g_{13}u_1 \\ 0 & 0 & 0 \end{bmatrix}. \tag{54}
$$

Since $g_{11}^2 + g_{12}^2 = 1$, at equilibrium we must have

$$
\begin{aligned}
u_2 &= u_1, \\
g_{11} &= 1 - g_{23}u_1, \\
g_{12} &= -g_{13}u_1.
\end{aligned} \tag{55}
$$

But equation (52) is also equivalent to

$$
\xi_2(g_e)g_e^{-1} = g_e^{-1}\xi_1(g_e), \tag{56}
$$

which (by an analogous computation) leads to

$$
\begin{aligned}
u_2 &= u_1, \\
g_{11} &= 1 - g^{23}u_2, \\
g_{12} &= g^{13}u_2.
\end{aligned} \tag{57}
$$

Using $g_{11}^2 + g_{12}^2 = 1$, from equation (55) we obtain

$$
\begin{aligned}
1 &= (1 - g_{23}u_1)^2 + g_{13}^2 u_1^2 \\
&= 1 - 2g_{23}u_1 + g_{23}^2 u_1^2 + g_{13}^2 u_1^2 \\
0 &= u_1 \left[\left(g_{13}^2 + g_{23}^2 \right) u_1 - 2g_{23} \right] \\
u_1 &= \frac{2g_{23}}{g_{13}^2 + g_{23}^2}, \quad \text{or } u_1 = 0.
\end{aligned} \tag{58}
$$

There are thus two distinct equilibrium cases to analyze: $u_1 = 0$ and $u_1 = 2g_{23}/r^2$. First, consider the case $u_1 = 0$. Then from equations (55) and (57), we conclude

$$
\begin{aligned}
u_2 &= u_1 = 0, \\
g_{11} &= 1, \\
g_{12} &= 0.
\end{aligned} \tag{59}
$$

26

For such an equilibrium, $\mathbf{x}_1 = \mathbf{x}_2$, so we also have

$$
\begin{aligned}
g_{13} &= -g^{13}, \\
g_{23} &= -g^{23}.
\end{aligned}
\tag{60}
$$

However, the relationship between $\mathbf{x}_1$ and $\mathbf{r} = \mathbf{r}_2 - \mathbf{r}_1$ is arbitrary.

Next, consider the case $u_1 = 2g_{23}/r^2 \neq 0$. We must assume that $r > 0$ so that u_1 is well-defined. Then from equations (55) and (57), we conclude

$$
\begin{aligned}
u_2 &= u_1 = 2g_{23}/r^2, \\
g_{23} &= g^{23}, \\
g_{13} &= -g^{13}, \\
g_{11} &= 1 - 2g_{23}^2/r^2, \\
g_{12} &= -2g_{13}g_{23}/r^2.
\end{aligned}
\tag{61}
$$

With some further calculation (see Appendix B), one can show that the corresponding relative equilibrium consists of the two vehicles moving on the same circular orbit, separated by a chord of fixed length.

The notion of *shape space* associated to a symmetry group is useful for describing the evolution of system (42) [4–6]. To summarize, equation (42) describes motion in the configuration space. The variable $g = g_1^{-1}g_2$ plays the role of a shape variable, and evolves on the (collision-free) shape submanifold $M_{shape} = M_{config}/G$. The reduced dynamics on shape space are given by equation (51). Equilibria g_e of the reduced dynamics correspond to equilibrium shapes. The configuration variables can be expressed in terms of the shape variable as

$$
(g_1, g_2) = (g_1, g_1 g),
\tag{62}
$$

and if $g = g_e$ (i.e., the shape is an equilibrium shape), then the trajectory in the configuration space is a relative equilibrium.

Remark: The collision-free submanifold M_{shape} is isomorphic to $\mathbb{R} \times \mathbb{T}^2$, the set which appears in the statement of **Proposition 1**. Indeed, **Proposition 1** can be understood as a convergence result for the shape dynamics. $\square$

Remark: The Lyapunov function V_{pair} given by equation (11) is, as expected, also G-invariant, and can be expressed as

$$
V_{pair} = -\ln\left[1 - (g_{13}g^{13} + g_{23}g^{23})/r^2\right] + h(r). \quad \square
\tag{63}
$$

7.2   The n-vehicle problem

The notions of configuration space and shape space described above for the 2-vehicle problem generalize naturally to n vehicles. The configuration space consists of n copies of $G = SE(2)$, and an appropriate non-collision manifold analogous to M_{config} can be defined. The dynamics in configuration variables can be expressed as

$$\dot{g}_1 = g_1\xi_1, \quad \dot{g}_2 = g_2\xi_2, \quad \dots \quad \dot{g}_n = g_n\xi_n, \tag{64}$$

where $\xi_1, \xi_2, \dots \xi_n \in \mathfrak{g}$ have the form

$$\xi_j = A_0 + A_1 u_j, \quad \forall j = 1, \dots, n. \tag{65}$$

We define the shape variables

$$\tilde{g}_j = g_1^{-1}g_j, \quad j = 2, \dots, n, \tag{66}$$

which evolve on the reduced (shape) space consisting of a product of $n - 1$ copies of G. (It is also possible to define shape variables in other combinations; e.g., $\tilde{g}_j = \tilde{g}_{j-1}^{-1}g_j$, $j = 2, \dots, n$ [5].) Here we have assumed that ξ_1, ξ_2, ... ξ_n depend only on the reduced variables $\tilde{g}_2, \tilde{g}_3, \dots \tilde{g}_n$ (and we note that this assumption can indeed be verified for the control law given by equation (36)).

By calculations analogous to those in the previous subsection, we are led to the conclusion that at equilibrium (in shape space),

$$u_1 = u_2 = \dots = u_n. \tag{67}$$

Proposition 3: Consider the dynamics given by equations (64) and (65), evolving on the collision-free submanifold

$$M_{config} = \left\{ (g_1, g_2, \dots, g_n) \in \overbrace{G \times G \times \dots \times G}^{n \text{ copies}} \, \middle| \, \mathbf{r}_{jk} = \mathbf{r}_k - \mathbf{r}_j \neq 0, \ 1 \leq j \neq k \leq n \right\}, \tag{68}$$

where $G = SE(2)$ (and $\mathbf{r}_j$ is defined as in equation (40) for $j = 1, \dots, n$). Assume that the controls $u_1, u_2, \dots u_n$ depend only on the shape variables given by equation (66) (i.e., the controls are G-invariant). Then for equilibrium shapes (i.e., for relative equilibria of the dynamics (64) on configuration space) $u_1 = u_2 = \dots = u_n$, and there are only two possibilities:

(a) $u_1 = u_2 = \dots = u_n = 0$ at equilibrium, in which case a relative equilibrium consists of all vehicles heading in the same direction (with arbitrary relative positions within the formation), or
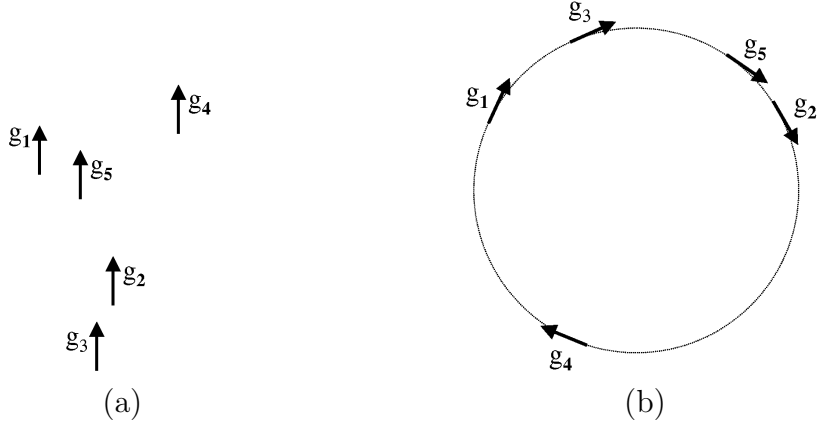
28

Fig. 12. Relative equilibria for the n-vehicle problem, illustrated for $n = 5$ (arrows indicate tangent vectors to the vehicle trajectories): (a) for $u_1 = u_2 = ... = u_n = 0$, and (b) for $u_1 = u_2 = ... = u_n \neq 0$.

(b) $u_1 = u_2 = ... = u_n \neq 0$, in which case a relative equilibrium consists of all vehicles moving on the same circular orbit, with arbitrary cordal distances between them.

Proof: Omitted due to space constraints, but essentially follows the same steps indicated in the previous subsection for the two-vehicle problem. $\square$

Figure 12 illustrates the two types of relative equilibria for the n-vehicle problem described in **Proposition 3**.

Thus, the control system (2), or system (36), can be naturally understood in the Lie group setting. This suggests that shape space notions for Lie groups may play an important role in formation control problems. We have shown how to characterize the set of all possible relative equilibria for *any choice* of G-invariant control law. We are now in the process of investigating the next obvious issue: how to choose controls that stabilize particular relative equilibria.

8   Conclusions and future research directions

Our work on formation control using models based on the Frenet-Serret equations of motion is still in its early stages. Areas of current and future work include developing control laws and proving stability results for formations of n vehicles, investigating continuum limits in which the number of "vehicles" becomes infinite, and investigating formation-control problems in the setting of the three-dimensional Frenet-Serret equations. On the practical side, there is also an effort underway to develop the hardware required for implementation of these types of control laws for meter-scale UAVs, and here the development

of the analog VLSI processor is one of the main challenges. An essential theme of this work is that *jointly* considering control law design and implementation issues has the best chance of ultimately leading to a prototype formation control system implementation for meter-scale UAVs.

9   Acknowledgements

References

[1] W.M. Boothby, *An introduction to differentiable manifolds and Riemannian geometry, 2nd ed.* Orlando: Academic Press, 1986.

[2] V. Jurdjevic, *Geometric Control Theory*, Cambridge: Cambridge University Press, 1997.

[3] H. Khalil. *Nonlinear Systems.* New York: Macmillan Publishing Co., 1992.

[4] R.G. Littlejohn and M. Reinsch, "Gauge fields in the separation of rotations and internal motions in the n-body problem," *Review of Modern Physics,* Vol. 69, No. 1, pp. 213-275, 1997.

[5] P.S. Krishnaprasad and D.P. Tsakiris, "G-Snakes: Nonholonomic Kinematic Chains on Lie Groups," *Proc. 33rd IEEE Conf. Decision and Control*, pp. 2955-2960, IEEE, New York, 1994. (see also Institute for Systems Research technical report ISR TR 94-27, 1994).

[6] F. Zhang and P.S. Krishnaprasad, "Center of Mass of a System of Particles in G" Preprint, 2002.

[7] L.-S. Wang and P.S. Krishnaprasad, "Gyroscopic control and stabilization," *Journal of Nonlinear Science*, Vol. 2, pp. 367-415, 1992.

[8] P. Ogren, E. Fiorelli, and N.E. Leonard, "Formations with a Mission: Stable Coordination of Vehicle Group Maneuvers," *Proc. MTNS*, to appear, 2002.

[9] J. Toner and Y. Tu, "Flocks, herds, and schools: A quantitative theory of flocking," *Phys. Rev. E*, Vol. 58, No. 4, pp. 4828-4858, 1998.

[10] H. Levine and W.-J. Rappel, "Self-organization in systems of self-propelled particles," *Phys. Rev. E*, Vol. 63, No. 1, pp. 017101-1 to 017101-4, 2000.

[11] A. Czirók, M. Matsushita, and T. Vicsek, "Theory of periodic swarming of bacteria: Application to *Proteus mirabilis*," *Phys. Rev. E*, Vol. 63, No. 3, pp. 031915-1 to 031915-11, 2001.

[12] E.W. Justh and F.J. Kub, "Analog CMOS High-Frequency Continuous Wavelet Transform Circuit," *Proc. IEEE Int. Symp. Circuits and Systems,* Vol. 2, pp. 188-191, 1999.

[13] D. Grünbaum, "Schooling as a strategy for taxis in a noisy environment," in *Animal Groups in Three Dimensions*, J.K. Parrish and W.M. Hamner, eds., Cambridge University Press, 1997.

Appendix A

Derivation of equation (13):

$$
\begin{aligned}
\sin(\phi_2 - \phi_1)&(\cos\phi_2 + \cos\phi_1) - (\cos(\phi_2 - \phi_1) + 1)(\sin\phi_2 - \sin\phi_1) \\
&= (\sin\phi_2\cos\phi_1 - \cos\phi_2\sin\phi_1)(\cos\phi_1 + \cos\phi_2) \\
&\quad -(\cos\phi_2\cos\phi_1 + \sin\phi_2\sin\phi_1)(\sin\phi_2 - \sin\phi_1) \\
&\quad -(\sin\phi_2 - \sin\phi_1) \\
&= \sin\phi_2\cos^2\phi_1 + \sin\phi_2\cos\phi_1\cos\phi_2 - \sin\phi_1\cos\phi_1\cos\phi_2 - \sin\phi_1\cos^2\phi_2 \\
&\quad - \sin\phi_2\cos\phi_1\cos\phi_2 - \sin^2\phi_2\sin\phi_1 + \sin\phi_1\cos\phi_1\cos\phi_2 + \sin^2\phi_1\sin\phi_2 \\
&\quad -(\sin\phi_2 - \sin\phi_1) \\
&= \sin\phi_2 - \sin\phi_1 - (\sin\phi_2 - \sin\phi_1) \\
&= 0.
\end{aligned}
\tag{69}
$$

Derivation of equation (14):

$$\sin(\phi_2 - \phi_1)\left(\sin(\phi_2 - \phi_1) + \frac{1}{2}(\sin 2\phi_2 - \sin 2\phi_1)\right)$$

$$= (\sin \phi_2 \cos \phi_1 - \cos \phi_2 \sin \phi_1)\Big[(\sin \phi_2 \cos \phi_1 - \cos \phi_2 \sin \phi_1)$$

$$+ (\sin \phi_2 \cos \phi_2 - \cos \phi_1 \sin \phi_1)\Big]$$

$$= \sin^2 \phi_2 \cos^2 \phi_1 - \sin \phi_1 \sin \phi_2 \cos \phi_1 \cos \phi_2$$

$$- \sin \phi_1 \sin \phi_2 \cos \phi_1 \cos \phi_2 + \sin^2 \phi_1 \cos^2 \phi_2$$

$$+ \sin^2 \phi_2 \cos \phi_1 \cos \phi_2 - \sin \phi_1 \sin \phi_2 \cos^2 \phi_2$$

$$- \sin \phi_1 \sin \phi_2 \cos^2 \phi_1 + \sin^2 \phi_1 \cos \phi_1 \cos \phi_2$$

$$= \cos \phi_1 \cos \phi_2 \left(\sin^2 \phi_1 - 2\sin \phi_1 \sin \phi_2 + \sin^2 \phi_2\right)$$

$$+ \cos^2 \phi_1 \left(\frac{1}{2}\sin^2 \phi_2 - \sin \phi_1 \sin \phi_2 + \frac{1}{2}\sin^2 \phi_1\right)$$

$$+ \cos^2 \phi_2 \left(\frac{1}{2}\sin^2 \phi_1 - \sin \phi_1 \sin \phi_2 + \frac{1}{2}\sin^2 \phi_2\right)$$

$$+ \frac{1}{2}\cos^2 \phi_1 \sin^2 \phi_2 - \frac{1}{2}\cos^2 \phi_1 \sin^2 \phi_1$$

$$+ \frac{1}{2}\cos^2 \phi_2 \sin^2 \phi_1 - \frac{1}{2}\cos^2 \phi_2 \sin^2 \phi_2$$

$$= \frac{1}{2}\Big[(\cos \phi_1 + \cos \phi_2)^2(\sin \phi_1 - \sin \phi_2)^2$$

$$+ \left(\cos^2 \phi_2 - \cos^2 \phi_1\right)\sin^2 \phi_1 + \left(\cos^2 \phi_1 - \cos^2 \phi_2\right)\sin^2 \phi_2\Big]$$

$$= \frac{1}{2}\Big[(\cos \phi_1 + \cos \phi_2)^2(\sin \phi_1 - \sin \phi_2)^2$$

$$+ \left(\cos^2 \phi_2 - \cos^2 \phi_1\right)\left(\sin^2 \phi_1 - \sin^2 \phi_2\right)\Big]$$

$$= \frac{1}{2}\Big[(\cos \phi_1 + \cos \phi_2)^2(\sin \phi_1 - \sin \phi_2)^2 + \left(\sin^2 \phi_1 - \sin^2 \phi_2\right)^2\Big]. \quad (70)$$

Appendix B

Here we show that the equilibrium equation (61), for $g_{23} \neq 0$, implies that the corresponding relative equilibrium consists of the two vehicles moving on the circular orbit, separated by a chord of fixed length. The first observation is that because $u_1 = u_2 = $ constant, both vehicles traverse circular orbits of

radius $1/|u_1|$. For the first vehicle, we define

$$Q_1 = \begin{bmatrix} \mathbf{x}_1 & \mathbf{y}_1 \end{bmatrix} \in SO(2), \tag{71}$$

so that

$$\dot{Q}_1 = Q_1 \begin{bmatrix} 0 & -u_1 \\ u_1 & 0 \end{bmatrix}, \tag{72}$$

which can be integrated with respect to time to give

$$Q_1(t) = Q_1(0) \begin{bmatrix} \cos(u_1 t) & -\sin(u_1 t) \\ \sin(u_1 t) & \cos(u_1 t) \end{bmatrix}. \tag{73}$$

The equation for $\mathbf{r}_1$, the position of the first vehicle as a function of time, becomes

$$\dot{\mathbf{r}}_1 = Q_1(0) \begin{bmatrix} \cos(u_1 t) \\ \sin(u_1 t) \end{bmatrix}, \tag{74}$$

which can be integrated with respect to time to give

$$\mathbf{r}_1(t) = \frac{1}{u_1} Q_1(0) \left(\begin{bmatrix} \sin(u_1 t) \\ -\cos(u_1 t) \end{bmatrix} + \mathbf{c}_1 \right), \tag{75}$$

where $\mathbf{c}_1$ is a constant vector. We thus obtain

$$\left\| \mathbf{r}_1(t) - \frac{1}{u_1} Q_1(0)\mathbf{c}_1 \right\|^2 = \left\| \frac{1}{u_1} Q_1(0) \begin{bmatrix} \sin(u_1 t) \\ -\cos(u_1 t) \end{bmatrix} \right\|^2 = \frac{1}{u_1^2}, \tag{76}$$

which shows that the trajectory of the first vehicle lies on a circle of radius $1/|u_1|$ centered at $(1/u_1)Q_1(0)\mathbf{c}_1$. Futhermore,

$$\mathbf{r}_1(0) = \frac{1}{u_1} Q_1(0) \left(\begin{bmatrix} 0 \\ -1 \end{bmatrix} + \mathbf{c}_1 \right). \tag{77}$$

The corresponding calculation for the second vehicle gives

$$\mathbf{r}_2(0) = \frac{1}{u_1} Q_2(0) \left(\begin{bmatrix} 0 \\ -1 \end{bmatrix} + \mathbf{c}_2 \right). \tag{78}$$

33

A relationship between $\mathbf{c}_1$ and $\mathbf{c}_2$ arises from the formula $g_2(t) = g_1(t)g$, where

$$
g = \begin{bmatrix} 1 - g_{23}u_1 & -g_{13}u_1 & g_{13} \\ g_{13}u_1 & 1 - g_{23}u_1 & g_{23} \\ 0 & 0 & 1 \end{bmatrix}
\tag{79}
$$

is the equilibrium shape. For convenience, we denote

$$
g = \begin{bmatrix} Q & \mathbf{b} \\ 0\ 0 & 1 \end{bmatrix},
\tag{80}
$$

and from $g_2(t) = g_1(t)g$, it follows that

$$
\begin{aligned}
Q_2(t) &= Q_1(t)Q, \\
\mathbf{r}_2(t) &= Q_1(t)\mathbf{b} + \mathbf{r}_1(t).
\end{aligned}
\tag{81}
$$

Then

$$
\begin{aligned}
\mathbf{r}_2(0) &= Q_1(0)\mathbf{b} + \mathbf{r}_1(0) \\
&= Q_1(0)\mathbf{b} + \frac{1}{u_1}Q_1(0)\left(\begin{bmatrix} 0 \\ -1 \end{bmatrix} + \mathbf{c}_1 \right) \\
&= Q_1(0)\left[\mathbf{b} + \frac{1}{u_1}\left(\begin{bmatrix} 0 \\ -1 \end{bmatrix} + \mathbf{c}_1 \right) \right],
\end{aligned}
\tag{82}
$$

and so

$$
\frac{1}{u_1}Q_2(0)\left(\begin{bmatrix} 0 \\ -1 \end{bmatrix} + \mathbf{c}_2 \right) = Q_1(0)\left[\mathbf{b} + \frac{1}{u_1}\left(\begin{bmatrix} 0 \\ -1 \end{bmatrix} + \mathbf{c}_1 \right) \right].
\tag{83}
$$

This leads us to conclude

$$
\mathbf{b} + \frac{1}{u_1}\left(\begin{bmatrix} 0 \\ -1 \end{bmatrix} + \mathbf{c}_1 \right) = \frac{1}{u_1}Q\left(\begin{bmatrix} 0 \\ -1 \end{bmatrix} + \mathbf{c}_2 \right).
\tag{84}
$$

Next, we make use of the specific form of g, namely

$$\mathbf{b} = \begin{bmatrix} g_{13} \\ g_{23} \end{bmatrix},$$

$$Q = \begin{bmatrix} 1 - g_{23}u_1 & -g_{13}u_1 \\ g_{13}u_1 & 1 - g_{23}u_1 \end{bmatrix}, \tag{85}$$

to observe that

$$\mathbf{b} + \frac{1}{u_1}\begin{bmatrix} 0 \\ -1 \end{bmatrix} = \frac{1}{u_1}Q\begin{bmatrix} 0 \\ -1 \end{bmatrix}. \tag{86}$$

Combining equations (84) and (86) then gives

$$\mathbf{c}_1 = Q\mathbf{c}_2. \tag{87}$$

The center of the circular orbit for the first vehicle was shown above to be $(1/u_1)Q_1(0)\mathbf{c}_1$, and likewise, the center of the circular orbit for the second vehicle is

$$\frac{1}{u_1}Q_2(0)\mathbf{c}_2 = \frac{1}{u_1}Q_1(0)Q\mathbf{c}_2 = \frac{1}{u_1}Q_1(0)\mathbf{c}_1. \tag{88}$$

Thus, the two vehicle trajectories traverse the same circle.

Note that the chordal distance between the vehicles is given by

$$r = \sqrt{g_{13}^2 + g_{23}^2}, \tag{89}$$

but the diameter of the circular trajectory is

$$d = \frac{2}{|u_1|} = \frac{g_{13}^2 + g_{23}^2}{|g_{23}|}. \tag{90}$$

Thus, $d = r$ if and only if $g_{13} = 0$.